H_∞ Phase Locking Control for Wave Induced Wake Mixing

Van Den Berg, Daniel; De Tavernier, Delphine; Van Wingerden, Jan Willem

DOI
10.23919/ACC60939.2024.10644677

Publication date
2024

Document Version
Final published version

Published in
Proceedings of the American Control Conference, ACC 2024

Citation (APA)
Van Den Berg, D., De Tavernier, D., & Van Wingerden, J. W. (2024). H_∞ Phase Locking Control for Wave Induced Wake Mixing. In *Proceedings of the American Control Conference, ACC 2024* (pp. 1051-1056). (Proceedings of the American Control Conference). IEEE. https://doi.org/10.23919/ACC60939.2024.10644677

2024 American Control Conference (ACC)
July 8-12, 2024. Toronto, Canada

$\mathcal{H}_\infty$ Phase Locking Control for Wave Induced Wake Mixing*

Daniel van den Berg[1], Delphine De Tavernier[2] and Jan-Willem van Wingerden[1]

***Abstract*— The dynamic induction control wake mixing strategy has the potential to increase the energy yield of floating wind farms. These floating turbines will be subjected to surface waves, caused by the wind, and swell. When dynamic induction control is applied in open-loop, the effect of second-order wave forces and dynamic induction control on the thrust force can be out-of-phase and have destructive interference. In this work, we propose a method to synchronize the dynamic induction control input to the effect of the second-order wave forces. This is achieved by formulating the synchronization problem within an $\mathcal{H}_\infty$ optimization framework and designing a controller that minimizes the difference between the effect of wave-induced thrust variation and thrust variation. Time domain simulations show that synchronization at a desired frequency can be achieved and that the overall performance of the dynamic induction control method can be enhanced.**

I. INTRODUCTION

Europe targets 480 GW of installed wind capacity (on- and offshore combined) by 2030 [1]. To achieve this wind energy companies need to find access to deeper waters, where 80% of the total European wind energy resources are located [2]. To access these energy resources, turbines will need to be placed in cost-effective large, *floating*, wind farms. However, when placed in large wind farms, wind turbines interact with the wakes of surrounding turbines resulting in an extensive reduction of the power production of the individual turbines [3], [4].

This interaction can be negated using wake mixing techniques such as dynamic induction control [5] (DIC) or dynamic individual pitch control [6]. Both methods use blade pitching to vary the thrust force of the turbine which results in a time-varying wind field behind the turbine. This time-varying wind field disturbs the wake such that it breaks down earlier increasing wind speeds in the wake and thus the power generation of downstream turbines in case of partial or full wake overlap.

When these techniques are applied to a floating wind turbine (FWT), it will cause the FWT to displace. For dynamic induction control, the frequency and amplitude at which the blades are pitched impacts the effectiveness of the wake mixing technique [7]. The work in Ref. [7] does not consider the existence of waves, which may affect wake-mixing as well.

When subjected to waves, an FWT will also exhibit additional movement. Typically, wave-induced movement is excited at frequencies in the order of 0.1 Hz [8], whereas typical excitation frequencies for wake mixing techniques are located around 0.01 Hz, depending on turbine size and ambient wind speed. However, when subjected to a wave field, large floating vessels undergo a low-frequency displacement due to second-order wave forces [9]. For the FWT considered in the work, the NREL 5 MW reference turbine [10] mounted on the OC4 semisubmersible platform [11], has this second-order motion around 0.01 Hz [12]. When the waves are aligned with the wind direction, the resulting second-order motion causes a varying relative wind speed for the wind turbine, resulting in a varying thrust force and thus a similar wake mixing effect as DIC.

This paper demonstrates that this phenomenon can be leveraged using closed-loop control to benefit wake mixing for FWTs. Specifically, the thrust force variation desired for wake mixing may be initiated and amplified by synchronizing the response caused by pitch actuation and wave motion in a closed-loop setting. Recently, similar synchronization work with the goal of reducing actuator loads has been carried out for the Helix wake mixing technique [13]. Phase synchronization, or phase locking, is not an uncommon problem within control, receiving attention in mainly the electrical engineering field [14], [15]. In that work, phase-locked loops are feedback loops that aim to track the phase of an input signal. However, control of phase-locked loops is based on reference tracking a phase target. In the case of an FWT, control needs to phase-lock with a disturbance effect: the thrust variation due to waves. To that end, the following contributions are presented in this work:

1) We propose a novel phase-locking controller based on a linear $\mathcal{H}_\infty$ framework.
2) We show how low-order linear models can be obtained using the predictor-based subspace identification (or PBSID$_{opt}$) method.
3) We demonstrate that we can derive a simple fixed order controller using the same framework.
4) We provide a first proof-of-concept of the proposed controller within a challenging novel application.

The remainder of this paper is organized as follows: Section II introduces a more detailed description of the problem, including the models which will be used for control design. The setup for control design is covered in Section III and includes a description of the generalized plant, the weights used and the final optimized closed-loop transfer functions. The synthesized controller is implemented in Section IV on a

*This project is part of the Floatech project. The research presented in this paper has received funding from the European Union's Horizon 2020 research and innovation programme under grant agreement No. 101007142.

[1]Delft Center for Systems and Control, Delft University of Technology, Mekelweg 2, 2628 CD Delft, The Netherlands d.g.vandenberg@tudelft.nl

[2]Department of Flow Physics and Technology, Delft University of Technology, Kluyverweg 1, 2629 HS Delft, The Netherlands.

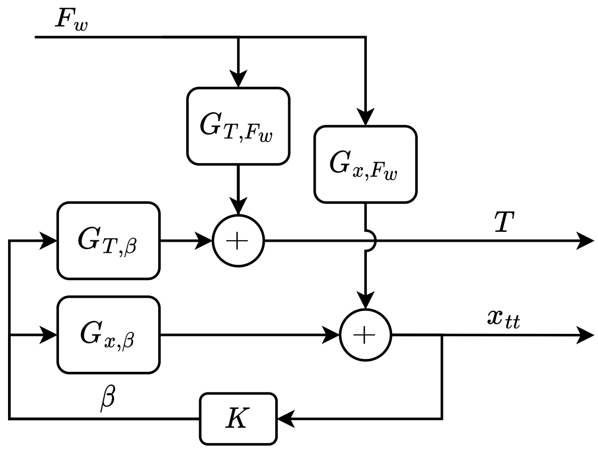

Fig. 1. Block diagram of a floating wind turbine with the relevant blocks and signals depicted.

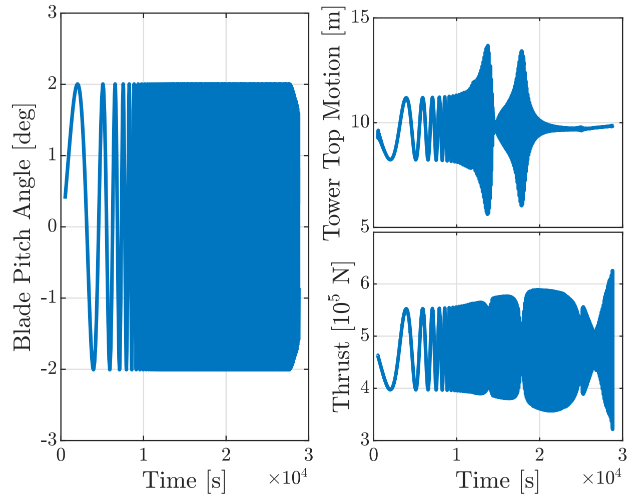

Fig. 2. Time domain data for chirp identification experiments.

linearized model of the FWT. Finally, Section V will contain the conclusion.

II. FLOATING WIND TURBINE MODEL

This section will give a description of the FWT model and describe the experiments for linear model identification. It will also give a brief summary of the PBSID$_{opt}$ method.

Figure 1 shows a block diagram of the floating wind turbine model and control signals. Each block represents a linear transfer function. The wave forces are represented by F_w. The translation of a wave force to the motion of the tower top, x_{tt}, is described by the model G_{x,F_w}, the effect of wave force on the turbine thrust, T, by G_{T,F_w}.

When closed-loop control is used, controller K will actuate blade pitching, β, to achieve synchronization. The input to the controller is the tower top motion since the thrust force of a (floating) wind turbine is difficult to measure, unlike the tower top displacement. Similar to the wave force, the effect of blade pitch on thrust and tower top motion is described by the models $G_{T,\beta}$ and $G_{x,\beta}$ respectively. The goal of the controller is to synchronize the outputs of G_{T,F_w} and $G_{T,\beta}$ such that they amplify each other. Since a linear control design technique will be used, linear models are required for the optimization. However, second-order wave forces are computed by solving quadratic transfer functions (QTFs) and are not easily translated to linear dynamics [9].

A. Identification Experiments

The non-linear dynamics are identified using excitation experiments. From the input-output relations linear models are identified. These experiments are conducted with a wind inflow speed of 9 m/s. Wake mixing is beneficial when turbines are operating in below-rated conditions [6]. Excitation frequencies which induce wake mixing are also wind speed dependent and can be characterized by the Strouhal number,

$$St = \frac{f_e D}{V}, \tag{1}$$

where f_e is the excitation frequency in Hertz, D the rotor diameter in meters and V the free stream wind speed in m/s. Numerical experiments indicate that a Strouhal between 0.15 and 0.50 results in wake mixing, where $St = 0.25$ is typically considered optimal for a two-turbine wind farm spaced at 5 rotor diameters [5]. For the NREL 5MW turbine, used in this work, with a rotor diameter of $D = 126$ m and wind inflow speed of 9 m/s, this Strouhal range translates to a frequency range of 0.011 to 0.036 Hz. It is therefore important that within this frequency range the linear models show good agreement with the non-linear dynamics. The excitation experiments are performed using QBlade [16], a simulation tool capable of simulating coupled aero- and hydrodynamics for floating wind turbines. For identification of $G_{T,\beta}$ and $G_{x,\beta}$ a chirp excitation signal is applied to the collective blade pitch input β. The chirp input is logarithmically distributed over the full duration, in total 8 hours of data, of the experiment and covers the frequency range from 1 mHz to 1 Hz. This frequency range is chosen such that it excites the dynamics of interest. The input and output data that will be used for identification are shown in Figure 2. From the time-domain data two resonance, and one anti-resonance can be seen in the tower top motion. Similar results are seen for the thrust data. For identification of G_{T,F_w} and G_{x,F_w}, an actual wave field is used as input. This wave field is defined using a Jonswap spectrum with a significant wave height $H_s = 1.5$, peak period $T_s = 8$ and gamma shape factor $\gamma = 1$. These values represent a wind-swept wave field for wind speeds around 9 m/s [17]. The second-order forces excite the system equally over a similar frequency range as that of the chirp input.

This can be seen in Figure 3, where the top graph shows the power spectral density of the wave input forces and the bottom graph shows the power spectra of the output signals. The power spectra of tower top motion as well as the turbine thrust two resonances can be identified. Furthermore, even though the input power of the waves is highest at 0.1 Hz, for this particular floating turbine equally dominant motions exist around 0.01 Hz, an order of magnitude lower.

B. System Identification Using the PBSID$_{opt}$ Method

For identification, the PBSID$_{opt}$ method is used [18]. This method constructs a predictor for a given state sequence. The system representation that forms the basis for the PBSID$_{opt}$ method is given by:

$$x_{k+1} = \tilde{A}x_k + \tilde{B}u_k + K_k y_k, \tag{2a}$$

$$y_k = Cx_k + Du_k + e_k. \tag{2b}$$

In (2a) and (2b) $\tilde{A} = A - K_k C$ and $\tilde{B} = B - K_k D$ with, $A \in \mathbb{R}^{n\times n}$, $B \in \mathbb{R}^{n\times n_u}$, $K_k \in \mathbb{R}^{n\times n_y}$, $C \in \mathbb{R}^{n_y\times n}$ and $D \in \mathbb{R}^{n_y\times n}$. The state, input, output and innovation signals are defined by the vectors $x_k \in \mathbb{R}^n$, $u_k \in \mathbb{R}^{n_u}$, $y_k \in \mathbb{R}^{n_y}$ and $e_k \in \mathbb{R}^{n_y}$ respectively. The Kalman gain is given by K_k. The system matrices can be retrieved by solving two least-squares problems:

$$X_{p+1,N_p-1} = \begin{bmatrix} A & B & K_k \end{bmatrix} \begin{bmatrix} X_{p,N_p-1} \\ U_{p,N_p-1} \\ E_{p,N_p-1} \end{bmatrix}, \tag{3a}$$

$$Y_{p,N_p} = \begin{bmatrix} C & D \end{bmatrix} \begin{bmatrix} X_{p,N_p} \\ U_{p,N_p} \end{bmatrix} + E_{p,N_p}. \tag{3b}$$

In (3a) and (3b) X_{p+1,N_p-1}, U_{p+1,N_p-1} and E_{p+1,N_p-1} represent block-row matrices, e.g.,

$$X_{p+1,N_p-1} = \begin{bmatrix} x_{p+1} & x_{p+2} & \dots & x_{p+N_p} \end{bmatrix}. \tag{4}$$

In (4) p is the past window, i.e., the number of data points on which the system will be identified and N_p is the number of data points in the data set. Solving (3a) and (3b) would require information on the full state sequence x_k, which is typically unavailable. It can, however, be reconstructed using an approach similar to the Observer/Kalman Filter Identification (OKID) method. This requires defining a new

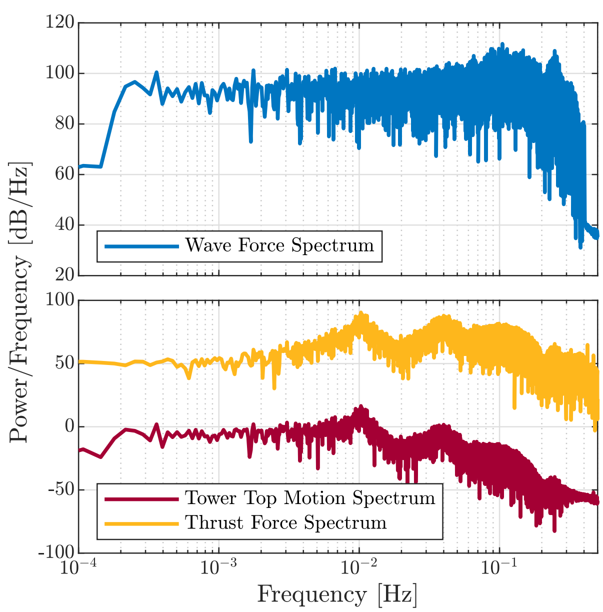

Fig. 3. Power spectra of input and output data for wave identification.

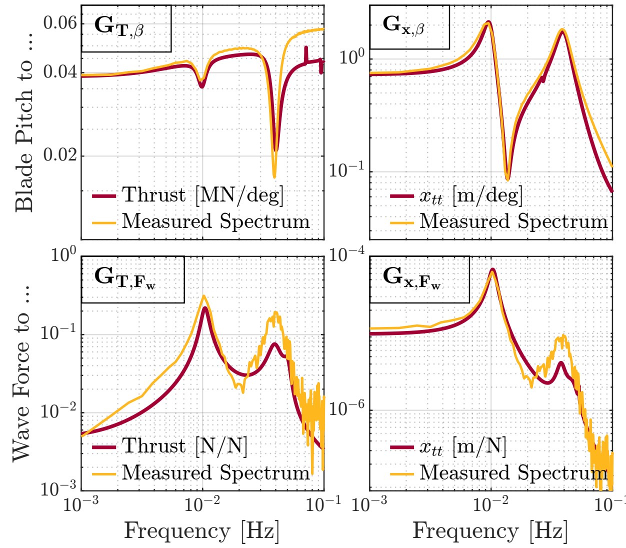

Fig. 4. Bode plots of the identified models with their respective identification spectra.

variable which is a column vector containing input and output data:

$$z_k = \begin{bmatrix} u_k \\ y_k \end{bmatrix},$$

and stacked vector over window p,

$$z_k^p = \begin{bmatrix} z_{k-p}^\top, & z_{k-p+1}^\top, & \dots, & z_{k-1}^\top \end{bmatrix}^\top.$$

State information can be reconstructed using a stacked data matrix Z_{0,p,N_p}, consisting of entries of z_k^p:

$$Z_{0,p,N_p} = \begin{bmatrix} z_p & z_{p+1} & \dots & z_{p+N_p-1} \\ z_{p-1} & z_p & \dots & z_{p+N_p-2} \end{bmatrix},$$

the extended observability matrix

$$\tilde{\Gamma}^f = \begin{bmatrix} C \\ C\tilde{A} \\ \vdots \\ C\tilde{A}^{f-1} \end{bmatrix}, \tag{5}$$

in which $f > n$ is the future window, and the extended controllability matrix $\tilde{\mathcal{K}}^p$:

$$\tilde{\mathcal{K}}^p = \begin{bmatrix} \tilde{A}^{p-1}\bar{B}, & \tilde{A}^{p-2}\bar{B}, & \dots, & \bar{B} \end{bmatrix}, \tag{6}$$

with $\bar{B} = \begin{bmatrix} \tilde{B}, & K_k \end{bmatrix}$. An estimate of X_{p,N_p} can then be found by solving a singular value decomposition

$$\tilde{\Gamma}^f X_{p,N_p} = \tilde{\Gamma}^f \tilde{\mathcal{K}}^p Z_{0,p,N_p} = \mathcal{U}_n \Sigma_n \mathcal{V}_n^\top, \tag{7}$$

The stacked state sequence, X_{p,N_p}, is retrieved as

$$X_{p,N_p} = \Sigma_n \mathcal{V}_n^\top. \tag{8}$$

Having reconstructed X_{p,N_p}, the original least-squares problems of (3a) and (3b) can be solved to find the system matrices.

The operating point chosen for identification is for a wind speed of 9 m/s. The working point blade pitch angle is such that the floating wind turbine extracts the maximum

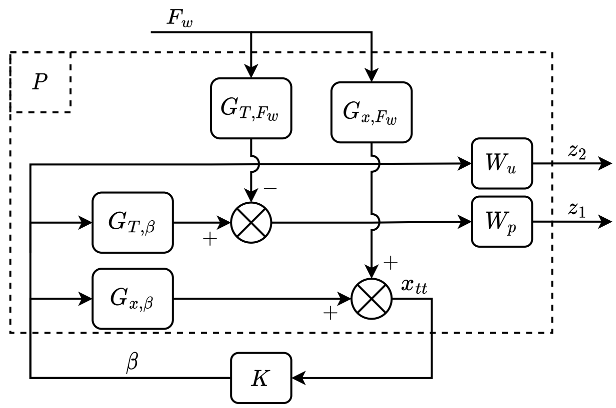

Fig. 5. Generalized plant with weights used in optimization.

energy from the flow. The resulting thrust, at this operating point, causes a surge and pitch displacement of the floater. These transients from the initialization of the simulation last around 500 seconds and are removed from the data set. The Bode plots of the identified models are shown in Figure 4. The settings for identification were chosen such that the linear models showed good agreement with their respective spectra in the frequency range of 0.010 to 0.035 Hz. These frequencies cover the range typically used for wake-mixing, and where second-order wave forces contain the most energy.

III. $\mathcal{H}_\infty$ CONTROL DESIGN

In this section, the $\mathcal{H}_\infty$ control design method is introduced. This control design method is chosen since closed-loop performance can easily be shaped by the design of performance weights. First, the FWT model given in Figure 1 will be expanded to a generalized plant for the synthesis problem. Second, the weights will be introduced and explained and finally, the results of the $\mathcal{H}_\infty$ synthesis will be shown and discussed. Based on this synthesis a low order fixed-structure controller is derived. This fixed-structure controller will be used for the simulations.

A. Generalized Plant

Figure 5 shows the FWT model of Figure 1 expanded to the generalized plant P required for the synthesis problem [19]. The disturbance caused by the wave force F_w is the only exogenous input signal to the system.

In this work, two performance signals are specified. The signal z_1 is defined as a weighted difference between the outputs of G_{T,F_w} and $G_{T,\beta}$. This performance signal is weighted by W_p aiming to minimize the difference between these two signals at a desired frequency. If this difference is driven to zero, the signal coming from the controlled block $G_{T,\beta}$ will have to be the same amplitude and exactly in phase with the disturbance signal, i.e., synchronization between the two signals. Performance signal z_2 is weighted by W_u, and is used to limit control action. The closed-loop transfer functions for which the controller will be optimized are:

$$N_1 = \frac{z_1}{F_w} = W_p\bigg(- G_{T,F_w} + \frac{G_{T,\beta} K G_{x,F_w}}{1 - G_{x,\beta}K}\bigg), \quad (9)$$

TABLE I

PARAMETERS USED FOR W_p AND W_u

Parameter	Value
K_w	20 [-]
ζ	0.01 [-]
ω_t	0.016 [Hz]
ω_b	0.064 [Hz]
K_u	$1 \cdot 10^6$ [-]

and

$$N_2 = \frac{z_2}{F_w} = W_u\bigg(\frac{K G_{x,F_w}}{1 - G_{x,\beta}K}\bigg). \quad (10)$$

Transfer function (9) represents the closed-loop transfer function from wave forces to performance channel z_1, which is the weighted channel used for synchronisation. Transfer function (10) is the weighted transfer function weighing the controller action.

B. Weight Design and Synthesis Results

The weight W_p is designed as an inverted damped notch. A damped notch filter is ideal for the suppression of a desired frequency. The general formula for W_p is

$$W_p = K_w \left(\frac{s^2 + 2\zeta s + \omega_t^2}{s^2 + \omega_b s + \omega_t^2}\right)^{-1}. \quad (11)$$

In (11) K_w is a constant that can be used to scale the weight, ζ is the damping factor, ω_t is the target frequency at which synchronization is desired and ω_b is the width of the notch. Weight W_u is designed as a second-order low-pass filter, aimed at suppressing control action at frequencies larger than the synchronization frequency. The weight W_u is given by:

$$W_u = K_u \frac{(s + \omega_t)^2}{(s + \omega_b)^2}. \quad (12)$$

The values given in Table I were used for the optimisation. The scaling factor K_u is large, primarily due to the difference in magnitude between second-order wave forces and blade pitch angle. The Robust Control Toolbox will be used in Matlab to solve the following $\mathcal{H}_\infty$ minimization problem:

$$\min_K ||N||_\infty, \;\; N = \begin{bmatrix} N_1 \\ N_2 \end{bmatrix}. \quad (13)$$

Figure 6 shows the results of the $\mathcal{H}_\infty$ synthesis for the closed-loop control problem. The inverse of weight W_p is also included in the figure. At the desired frequency, ω_t, the closed-loop transfer function follows the weight. This implies that the controller will bring any difference between the signals from the outputs of G_{T,F_w} and $G_{T,\beta}$ to zero. The roll-off that starts at 0.1 Hz is due to the design of weight W_u, limiting control action beyond that frequency.

C. Low Order Fixed-Structure Controller

The synthesized $\mathcal{H}_\infty$ controller is of high order and typically unsuited to being deployed in an uncertain or non-linear system. The order can be reduced by designing a lower-order fixed-structure controller that has a gain only at the synchronization frequency and achieves the required

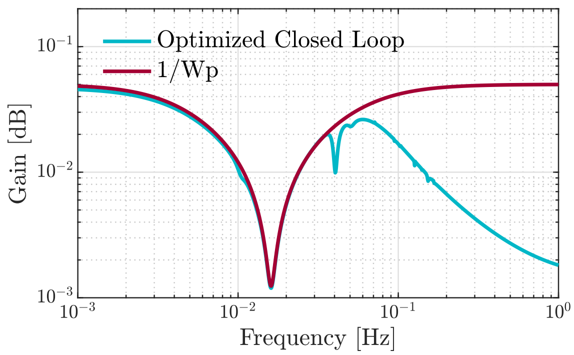

Fig. 6. Optimized closed-loop transfer function compared to weight W_p^{-1}.

phase delay. This lower-order controller is designed to be an inverted notch filter:

$$K_f = K_s \frac{s^2}{s^2 + \beta_f \omega_f s + \omega_f^2} \frac{\omega_{lp}}{(s + \omega_{lp})^2}, \quad (14)$$

in which K_s is constant gain, β_f the damping factor, ω_f the frequency of the inverted notch and ω_{lp} is the filter frequency for the low pass filter.

The low pass filter is added to reduce sensitivity to first-order wave movements. An inverted notch is chosen because of its predictable and tunable phase behaviour as well as having high gain at its phase drop. The notch frequency, ω_f, is based on the phase of the $\mathcal{H}_\infty$ controller at the synchronization frequency. The damping factor, β_f, can be used to change the frequency sensitivity of the fixed-structure controller; the smaller the damping factor the narrower the peak of the notch and vice versa. The Bode plots of both controllers are given in Figure 7.

IV. EVALUATION ON LINEAR FWT MODEL

This section will evaluate the controller in time-domain simulations. The simulations are carried out in Simulink, using the linear models developed in Section II.

The fixed-structure controller is implemented in the closed-loop model from Figure 1. The performance of the closed-loop system is compared to the open-loop implementation of dynamic induction control. The open-loop data is generated by setting a sinusoidal input directly on the blade pitch input of $G_{T,\beta}$ and $G_{x,\beta}$. Both the open- and the closed-loop systems will be excited with the same disturbance input. In this work, the second-order wave forces are represented using a cosine wave of appropriate amplitude on which a sine wave with a smaller amplitude and higher frequency is superimposed. This higher frequency sine wave represents the system being excited by the first-order waves. The frequency for both the open-loop implementation and the disturbance forces are set at ω_t. This simplified input is chosen to focus on the performance of the synchronization controller.

The blade pitch amplitude in the open-loop simulation is chosen to be in line with the control action of the closed-loop controller. The chosen phase difference between the open-loop input and second-order wave forces represents a worst-case scenario, i.e., the influence of the waves is almost entirely out of phase with the thrust variation due to blade pitch. The time domain results, during steady-state operation, are shown in Figure 8. The controller achieves synchronisation with the low-frequency thrust variations, using the tower top displacement as input. The synchronization of the outputs of $G_{T,\beta}$ and G_{T,F_w} results in an increase in the thrust variation. This contrasts with the open-loop results, which show what can happen when the effect of these particular waves is left unaccounted for. With the signals almost completely out of phase with each other, the resulting thrust variation is reduced.

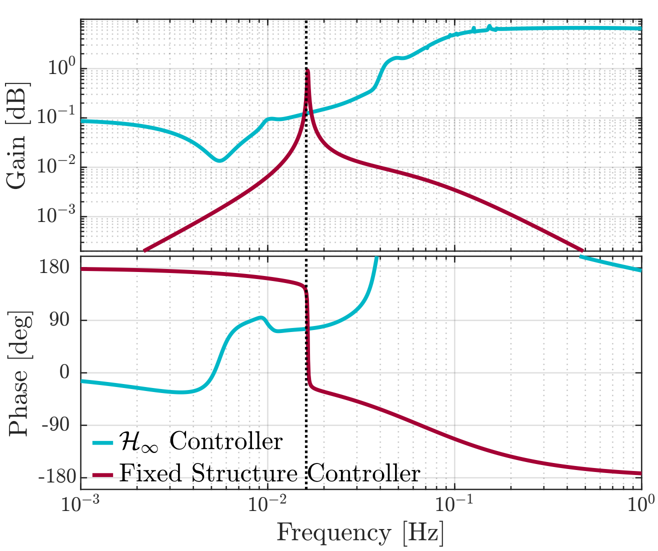

Fig. 7. Comparison of the full $\mathcal{H}_\infty$ controller with the fixed structure controller K_f.

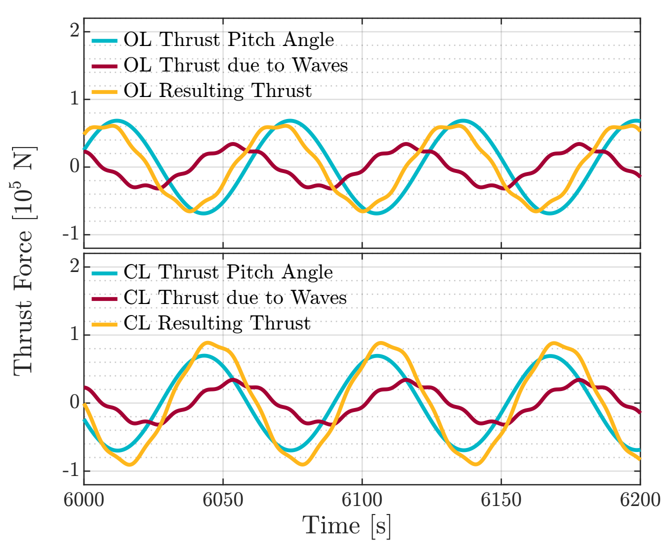

Fig. 8. Comparison of open-loop simulation (top figure) to closed-loop simulation (bottom figure).

V. CONCLUSION

This work proposes a novel method using the $\mathcal{H}_\infty$ optimization framework to design controllers that achieve synchronization between two signals. Linear models were developed of a floating wind turbine using the PBSID$_{opt}$ method. These linear models were implemented within a generalized plant and used in $\mathcal{H}_\infty$ synthesis. By changing the disturbance input contribution from additive to subtractive within the generalized plant the synthesized controller is designed for synchronization with the disturbance effect. Time domain simulations show that synchronization can be achieved by the optimized controller with an increase in thrust force variation as a result.

This work is a proof-of-concept of how $\mathcal{H}_\infty$ synthesis can be used to achieve synchronization. The controller is implemented within a linear representation of the FWT and the simulation is an idealized scenario with a single sinusoidal wave input signal and is very much a showcase of the synchronization methodology.

REFERENCES

[1] European Commission, *Information on the REPowerEU initiative.* https://ec.europa.eu/info/strategy/priorities-2019-2024/european-green-deal/repowereu-affordable-secure-and-sustainable-energy-europe_en, 2022.

[2] WindEurope, *Floating Offshore Wind Vision Statement*, https://windeurope.org/about-wind/reports/floating-vision-statement/, 2017.

[3] R. J. Barthelmie, S. C. Pryor, S. T. Frandsen, K. S. Hansen, J. G. Schepers, K. Rados, W. Schlez, A. Neubert, L. E. Jensen, and S. Neckelmann, "Quantifying the Impact of Wind Turbine Wakes on Power Output at Offshore Wind Farms," *Journal of Atmospheric and Oceanic Technology*, vol. 27, no. 8, pp. 1302–1317, 2010, Publisher: American Meteorological Society Section: Journal of Atmospheric and Oceanic Technology.

[4] J. Meyers, C. Bottasso, K. Dykes, P. Fleming, P. Gebraad, G. Giebel, T. Göçmen, and J. W. van Wingerden, "Wind farm flow control: Prospects and challenges," *Wind Energy Science*, vol. 7, no. 6, pp. 2271–2306, 2022.

[5] W. Munters and J. Meyers, "Towards practical dynamic induction control of wind farms: Analysis of optimally controlled wind-farm boundary layers and sinusoidal induction control of first-row turbines," *Wind Energy Science*, vol. 3, pp. 409–425, 2018.

[6] J. A. Frederik, B. M. Doekemeijer, S. P. Mulders, and J. W. van Wingerden, "The helix approach: Using dynamic individual pitch control to enhance wake mixing in wind farms," *Wind Energy*, vol. 23, no. 8, pp. 1739–1751, 2020.

[7] D. G. van den Berg, D. De Tavernier, and J. W. van Wingerden, "The Dynamic Coupling Between the Pulse Wake Mixing Strategy and Floating Wind Turbines," *Wind Energy Science Discussions*, vol. 2023, pp. 1–23, 2023.

[8] K. Hasselmann, T. P. Barnett, E. Bouws, H. Carlson, D. E. Cartwright, K. Enke, J. Ewing, A. Gienapp, D. Hasselmann, P. Kruseman, *et al.*, "Measurements of wind-wave growth and swell decay during the Joint North Sea Wave Project (JONSWAP).," *Ergaenzungsheft zur Deutschen Hydrographischen Zeitschrift, Reihe A*, 1973.

[9] J. M. J. Journée, W. W. Massie, and R. H. M. Huijsmans, "Offshore Hydromechanics Third Edition," 2015.

[10] J. Jonkman, S. Butterfield, W. Musial, and G. Scott, "Definition of a 5-MW Reference Wind Turbine for Offshore System Development," Feb. 2009.

[11] A. Robertson, J. Jonkman, M. Masciola, H. Song, A. Goupee, A. Coulling, and C. Luan, "Definition of the Semisubmersible Floating System for Phase II of OC4," Sep. 2014.

[12] I. Bayati, J. Jonkman, A. Robertson, and A. Platt, "The effects of second-order hydrodynamics on a semisubmersible floating offshore wind turbine," in *Journal of Physics: Conference Series*, IOP Publishing, vol. 524, 2014, p. 012 094.

[13] A. A. W. van Vondelen, J. Ottenheym, A. K. Pamosoeuryo, S. T. Navalkar, and J. W. van Wingerden, "Phase synchronization for helix enhanced wake mixing in downstream wind turbines," 2, 22nd IFAC World Congress, vol. 56, 2023, pp. 8426–8431.

[14] F. Gardner, "Charge-pump phase-lock loops," *IEEE transactions on Communications*, vol. 28, no. 11, pp. 1849–1858, 1980.

[15] R. E. Best, *Phase-locked loops: design, simulation, and applications*. McGraw-Hill Education, 2007.

[16] D. Marten, "QBlade: A modern tool for the aeroelastic simulation of wind turbines," Ph.D. dissertation, Technische Universität Berlin, 2020.

[17] C. Allen, A. Viselli, H. Dagher, A. Goupee, E. Gaertner, N. Abbas, M. Hall, and G. Barter, "Definition of the UMaine VolturnUS-S Reference Platform Developed for the IEA Wind 15-Megawatt Offshore Reference Wind Turbine," Jul. 2020.

[18] G. van der Veen, J. W. van Wingerden, M. Bergamasco, M. Lovera, and M. Verhaegen, "Closed-loop subspace identification methods: An overview," *IET Control Theory & Applications*, vol. 7, no. 10, pp. 1339–1358, 2013.

[19] S. Skogestad and I. Postlethwaite, *Multivariable feedback control: analysis and design*. John Wiley & Sons, 2005.